

Quasiparticles and Band Transport in Organized Nanostructures of Donor-Acceptor Copolymers

Guorong Weng and Vojtěch Vlček*

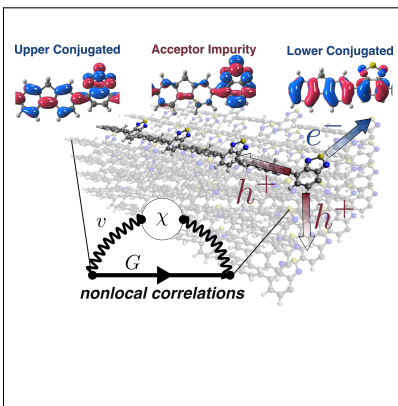
*Department of Chemistry and Biochemistry, University of California, Santa Barbara,
93106, U.S.A*

E-mail: vlcek@ucsb.edu

Abstract

The performance of organic semiconductor devices is linked to highly-ordered nanostructures of self-assembled molecules and polymers. We employ many-body perturbation theory and study the excited states in bulk copolymers. We discover that acceptors in the polymer scaffold introduce a, hitherto unrecognized, conduction impurity band. The donor units are surrounded by conjugated bands which are only mildly perturbed by the presence of acceptors. Along the polymer axis, mutual interactions among copolymer strands hinder efficient band transport, which is, however, strongly enhanced across individual chains. We find that holes are most effectively transported in the $\pi - \pi$ stacking while electrons in the impurity band follow the edge-to-edge directions. The copolymers exhibit regions with inverted transport polarity, in which electrons and holes are efficiently transported in mutually orthogonal directions.

Graphical TOC Entry



Keywords

Organic semiconductor, quasiparticle excitations, donor-acceptor copolymer, impurity states, band transport, many-body interactions

Donor-acceptor (D-A) semiconducting copolymers represent arguably the most variable class of semiconducting materials in organic electronics.¹⁻⁴ The wide range of possible donors and acceptors provides an unmatched tunability of the system’s electronic and optical properties.⁵⁻⁷ Rational device-design is, however, hampered by the complicated relationship between electronic properties and the arrangement of the molecular chains in the condensed phase (e.g., in spin-coated thin-films).^{8,9} Experiments showed that highly-ordered *nanodomains*, i.e., highly organized nm-scale regions, are widely present in solution-processed thin films. The nanodomains are composed of nanowires,¹⁰ nanosheets,¹¹ and crystallites.¹²⁻¹⁵ Face-on (π - π) or edge-on stacking is the dominant arrangement of conjugated molecules leading to high charge mobilities and excellent device performance.¹⁰⁻¹⁵ The nanodomains exhibit quasiparticle bands observed by angle-resolved photoemission.¹⁶ Hence, the high hole mobilities are explained by band-like transport^{17,18} in the π - π direction.^{12,14,19} However, a detailed microscopic understanding of how the structure and composition of the copolymers impact the electronic excitations is currently missing.

Answering these questions requires a theoretical investigation of the copolymers’ electronic structure in the condensed phase. In principle, such simulations need to capture the non-local inter-molecular interactions²⁰ of electrons delocalized along the π -conjugated backbone.¹⁶ The individual polymer chains are highly polarizable and held together by van der Waals (vdW) forces. Even in the limit of ideally crystalline systems, quantitative theoretical predictions of electronic excitations are prohibitive, and they have been limited to crystals of small molecules.²¹⁻³¹ For polymers, the computational efforts have considered only isolated^{32,33} oligomers or 1D periodic systems³⁴⁻³⁸ treated by mean-field approaches, which are less expensive but do not take into account the non-local electronic correlations (governed by polarization effects).³⁹ Further, the geometries of the polymer strands are typically forced to be planar, i.e., they disregard actual arrangements in the highly organized domains.^{33,37} Finally, the mean-field methods do not, in principle, provide access to quasiparticle (injected electron and hole) energies and tend to underestimate excitation energies grossly.⁴⁰

In this work, we overcome these limitations and apply state-of-the-art theoretical approaches to explain the key features of the electronic structure of D-A copolymers. Our calculations employ many-body perturbation theory⁴⁰ within the stochastic *GW* approach.^{41–44} The electron-electron interactions are computed for each excitation (i.e., no mean-field approximation is applied). In the *GW* approximation, the interaction term takes into account a selected class of Feynman diagrams describing the electrodynamic screening, i.e., the induced charge density fluctuations. Electrons thus interact via a screened Coulomb interaction, which is non-local and time-dependent. In practice, the *GW* method yields quasiparticle (QP) excitation energies in excellent agreement with available experimental data.^{40,42,45}

The electronic structure and QP energies of the condensed phase is determined by the properties of the constituting moieties as well as by mutual interactions among individual copolymer strands. While these contributions are nontrivial, relations among a few key parameters govern the system’s overall behavior. To illustrate this, we consider a prototypical example: “FBT” and related D-A copolymers^{46–48} (see Supporting Information (SI) for the geometry optimization). Here, the fluorene moiety (F) acts as a “donor” (D), and benzothiadiazole (BT) acts as an “acceptor” (A). The isolated molecules are illustrated in the inset of **Figure 1** and the SI. The D units are the source of delocalized electronic states. In contrast, acceptors are typically chosen so that they have a higher electron affinity than donors,^{49,50} acting as strong potential wells for electrons (see **Figure ??**). Hence, the A unit is a source of localized electrons whose wave functions have a limited spatial extent.

In a single copolymer strand (i.e., 1D periodic system with repeated D and A subunits), the quantum confinement is reduced in the direction of the polymer axis. Consequently, the fundamental gap of the infinite chain decreases with the polymerization length; for an infinite system, it is 4.08 ± 0.04 eV, which is 1.48 ± 0.05 eV less than for an isolated monomer (**Figure ??**). In a condensed phase (either 2D slab or 3D bulk), the presence of neighboring strands eliminates the quantum confinement in the directions orthogonal to the polymer axis. Hence, the fundamental band gap further decreases (Figure ??b).

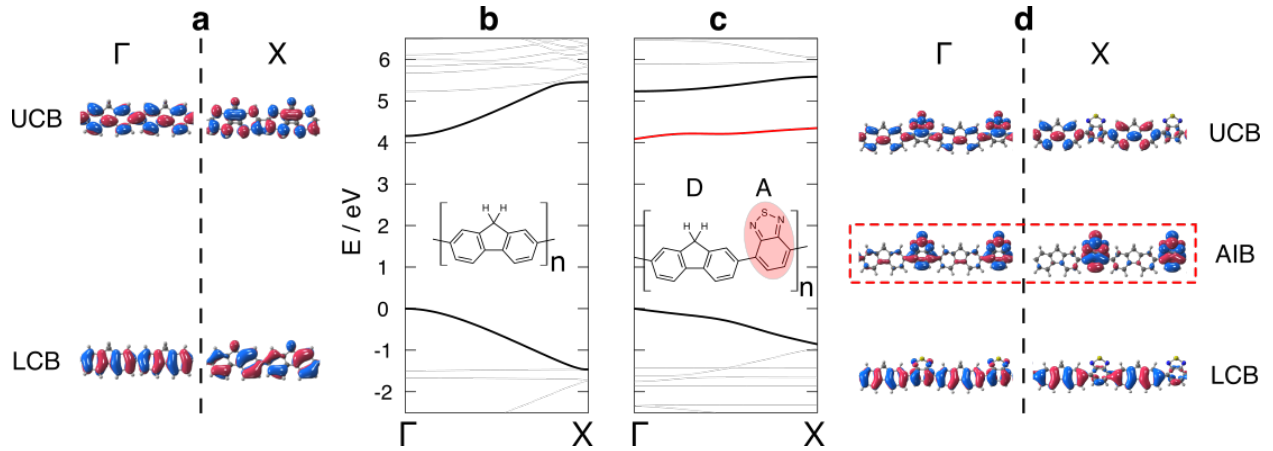


Figure 1: Quasiparticle band structures and orbitals of selected states of a fluorene (a, b) and FBT (c, d) strands. The monomer units are shown in the inset of panels b and c. The electronic states that are delocalized over the entire polymer backbone are denoted lower and upper conjugated bands (LCB and UCB), for the highest valence and lowest conduction band. The band-edge states in fluorene (a) are formed by LCB and UCB illustrated for the Brillouin zone center, Γ , and its boundary, X. The corresponding bands are highlighted in panel b. FBT is D-A copolymer, with the individual subunits labeled in the inset of panel c. Due to the presence of A, the bandstructure contains an acceptor impurity band (AIB) highlighted in red (c). Panel d depicts LCB, AIB, and UCB for two points in the Brillouin zone; the AIB is strongly localized on the acceptor subunit. Red and blue colors distinguish the wave function phase.

For quantitative predictions of the band gaps in the condensed phase, many-body methods turn out to be indispensable as dynamical electron-electron interactions are responsible for the non-local (inter-chain) interactions. Indeed, the ionization potential for the 2D slab computed with the *sGW* method is 5.48 ± 0.02 eV (Figure ??a), in excellent agreement with thin-film experiments that provide an estimate of 5.4-5.5 eV.⁴⁷ The fundamental band gaps of the surface and the bulk are 3.33 and 2.23 eV (Figure ??b), and the latter is in good agreement with the experimental value of 2.32-2.44 eV.⁴⁷

The periodic copolymer arrangement supports the formation of band structures (observed experimentally, as discussed above). To characterize the principal features of the electronic states, we start with the 1D system shown in Figure 1c. The crystal momentum is imprinted on the individual wavefunctions (Figure 1d), which, however, retain much of their molecular character (**Figure ??**). It is thus possible to separate the contributions of D and A to the highest valence and lowest conduction bands responsible for the charge transport.

The donor behavior dominates the highest valence state; it has conjugated character and delocalized π orbitals (see more details in **Figure ??**). The top valence band is broad (its bandwidth is 0.86 ± 0.04 eV) with a parabolic dispersion near the extrema that occur at the critical points of the Brillouin zone. The near-band-edge character, together with the large bandwidth, translates to a low effective mass of $\sim 0.22m_e^*$. Such a low value is consistent with experimental results for similar (semi)conducting copolymers.¹⁶ We denote the highest conduction band and the lower conjugated band (LCB). The complementary “upper” conjugated band (UCB) is formed from π^* orbitals, and it has much higher energy (Figure 1d). Both LCB and UCB are qualitatively analogous to the band edge states in a *pure* fluorene chain (Figure 1a), i.e., the conjugated bands are only mildly perturbed by the presence of acceptor subunits. The correspondence between the electronic structures of D-A and pure donor polymers has not been noticed up to now.

In contrast, the lowest conduction band of the copolymer comprises states localized only on the acceptors (Figure ??). The acceptor band has significantly reduced width (Figure 1c),

and it appears between LCB and UCB.

In calculations with distinct A molecules, we found that the exact energy separation between the conjugated and localized states depends only a little on the choice of acceptors (see **Figure ??** for details). In FBT, the separation of the conduction states is 1.11 eV; the oxygen- and selenium- substituted copolymers show slightly larger separations (1.38 eV and 1.16 eV, respectively – see **Figure ??**). In all cases studied, the localized state is characteristically inserted between the two conjugated bands. Based on the conceptual analogy to charge-trapping “in-gap” states, we denote the lowest conduction states as the acceptor impurity band (AIB). The formation of the localized and flat impurity band has not been described previously. One of the key findings of this communication is the recognition and distinction between the conjugated and impurity bands.

LCB, AIB, and UCB are present in the same order in 1D and in the condensed phases. While the van der Waals forces only weakly bond the individual copolymer strands, the inter-chain interactions change the band structures significantly. Besides the shift of the QP gaps (discussed above), the charge transport is critically influenced by the changes in the bandwidth. The dispersion of LCB and AIB determines the charge transport polarity. Further, the bandwidth is directly related to the charge carrier effective mass. To investigate the physical origin of the of the band structure changes, we will separate two main contributions: (i) the one-body electronic interactions⁵¹ including the (classical) density-density Coulomb repulsion (**Table ??**), and (ii) the electron-electron interactions, which represent highly non-local and dynamical (time-dependent) quantum effects.

The first contribution mostly depends on the local⁵² properties of the copolymer. The electronic structure (and charge transport) strongly depend on the bond arrangement between the donor and acceptor subunits.³⁵ The existence of a single bond between adjacent donors and acceptors implies large rotational freedom. In practice, the mutual orientation of the A and D units depends on the environment. The rotational angle varies between 43° and 56° in the relaxed structures with 1D, 2D, or 3D topology (**Figure ??**). Other structural

variations are insignificant as the rest of the copolymer backbone is rigid, and we disregard them in the analysis.

As noted above, AIB is composed of localized states centered on the acceptor subunits. The corresponding wave function near the conduction edge does extent to the D-A joint appreciably (Figure 1d). Hence, AIB is practically insensitive to the torsion angle. In contrast, rotation away from the ideally planar geometry leads to the narrowing of conjugated states (**Figure 2b**). Since the torsion angle is larger in the condensed phase than in a free-standing polymer, the hole effective mass in LCB is thus increased in bulk compared to a prediction from the 1D model.

The sensitivity of LCB is directly related to the character of the wave function near the D-A bond. Going from the low energy part of the LCB (near the X point of the Brillouin zone) to the band edge, the wavefunction develops a nodal plane across the D-A joint (Figure 2c). The presence of the nodes is associated with increased QP kinetic energy. A close inspection of various torsion angles reveals that the nodes across the D-A bond are suppressed when going from 1D to 3D conformation. The band edge is kinetically stabilized (Figure 2a), while the bottom LCB is insensitive to the rotation. As a result, the single-electron interactions promote bandwidth reduction in the condensed phase.

While the local properties are clearly responsible for the electronic structure modification, the non-local many-body effects are equally important and influence the excited states. These electron-electron interactions are decomposed into two principal contributions: (i) non-local exchange (due to the fermionic nature of the charge carriers), and (ii) time-dependent correlations among electrons and holes (which include vdW interactions responsible for the cohesive energy of the bulk). The significance of the many-body treatment is illustrated by the fact that LCB and AIB widths increase by $\sim 25\%$ and $\sim 46\%$ if the non-local and dynamic description is used instead of the common mean-field approach (e.g., in local and static density functional theory – see **Table ??**).

We first inspect the behavior of the conjugated states. While the exchange interaction

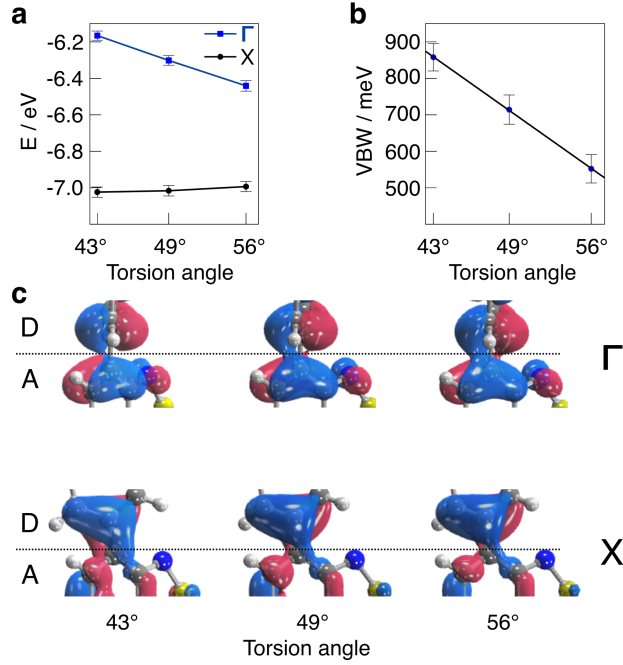


Figure 2: The effect of the characteristic torsion angles between D and A subunits found in various condensed phases of FBT: (a) The QP energies of LCB at the Brillouin zone center, Γ , and its boundary, X as a function of the torsion angle. The QP energy of LCB is more sensitive to torsion at Γ than that at X. (b) The QP valence bandwidth linearly decreases with the torsion angle. (c) The LCB wavefunction at the donor (D) and the acceptor (A) joint for Γ and X points of the Brillouin zone. Red and blue colors distinguish the wavefunction phase. At Γ , the torsion gradually destroys a nodal plane between D and A, leading to kinetic stabilization of the QP energy. Conversely, the “bridging character” of LCB at the X point is little affected by the increased torsion. The error bars in panels a and b represent the statistical error of the stochastic many-body calculation.

typically drives electron localization,⁵³ it surprisingly enhances the dispersion of the delocalized bands along the polymer axis. The energies of states near the valence band maximum are stabilized much less than at the Brillouin zone boundary, i.e., the X-point (**Figure ??a**). In the latter case, there is an increased spatial overlap with a large number of occupied orbitals, and energy decrease is observed for states near the X-point. The exchange-driven band widening is a signature of the conjugated bands, and it is not observed otherwise. To document this, we provide complementary calculations for additional polymer strands (polyacetylene and polyethylene, with and without conjugated bonds) in the SI (**Table ??**).

In general, this effect is dramatic for copolymer systems. In the absence of electronic correlation (which reduces the exchange through dynamical screening), LCB would widen by an additional 40%. This increase can be paralleled with a (spurious) infinite-range response to hole localization observed for bare exchange interactions.⁵⁴

The screening contribution thus changes the picture qualitatively. It is governed by the reducible polarizability which is directly related to charge density fluctuations.⁴⁰ These correlation effects are dominated by optical (plasmon) excitation that shifts to lower energy as the crystal momentum increases (**Figure ??**). The states away from the band edge (i.e., closer to the Brillouin zone boundary) have energies approaching the resonant frequency of the collective charge density oscillations. For the corresponding quasiparticle excitations, the exchange interaction is strongly attenuated and becomes short range; the QP energies shift up, and the LCB consequently narrows (**Figure ??b**).

In the condensed systems, the LCB and UCB remain delocalized only along the polymer, not across the individual strands (illustrated in **Figure 3c**). As a result, the conjugated bands can further flatten. Along the edge-to-edge direction ($\Gamma \rightarrow Z$ **Figure 3a**), both LCB and UCB are extremely narrow and effectively “molecular” in nature. Neither non-local exchange nor correlation effects contribute significantly to the quasiparticle energies in this case. In practice, any band-transport of holes in LCB is significantly hampered along the edge-to-edge stacking direction.

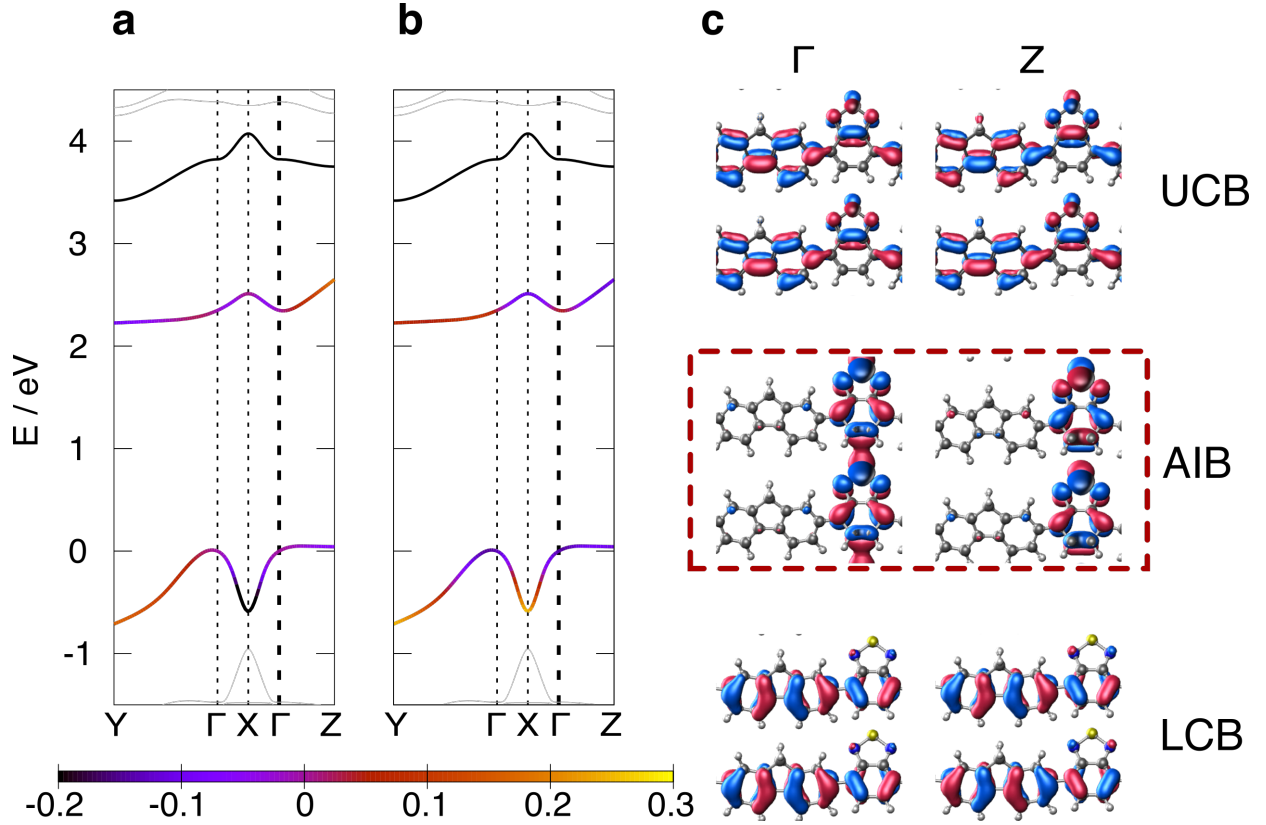


Figure 3: Quasiparticle band structure of FBT in a 3D crystalline domain with relative contributions of electronic (a) exchange and (b) correlation energies for LCB and AIB. The contributions are given by the color code and are plotted relative to the band average. The $\Gamma \rightarrow Y$ branch corresponds to the band in the π - π stacking direction; the $\Gamma \rightarrow X$ and $\Gamma \rightarrow Z$ branches correspond to the intra-chain and edge-on stacking directions. The inverted polarity regime is in the $\Gamma \rightarrow Z$, where the band dispersion of AIB is much higher than for the conjugated bands. (c) Local wave function character is of the selected states at two distinct points in the Brillouin zone along the $\Gamma \rightarrow Z$ direction. The two molecules are depicted in the edge-on stacking. Both LCB and UCB remain localized on individual strands, but AIB bridges the polymer chains. Red and blue colors distinguish the wave function phase.

However, the localization does not imply that the conjugated bands behave as those in an isolated strand. Here, the band dispersion is reduced by as much as 60% along the polymer axis compared to a free-standing copolymer. The flattening is most prominent in the 2D case (**Table ??**). Non-local interchain correlations govern the decrease of the LCB width; they are almost twice as big as the effect of torsion between the D and A subunits. In slabs, the strong polarization effects lead to the formation of local maxima in LCB and dispersion narrowing near the Γ point (**Figure ??b**). This indicates that in near-surface regions, the valence band-edge may not be characterized by a single crystal momentum vector, and the fundamental band-gap is likely indirect.

In contrast, cooperative interchain interactions appear along the $\pi - \pi$ stacking ($\Gamma \rightarrow Y$ in Figure 3). As a result, the LCB dispersion is the largest along this face-on direction (up to 710 meV). Significant bandwidth suggests a high propensity for efficient band-like transport of holes within LCB. The reason for the increased bandwidth (despite the strong on-chain localization) is twofold: first, the packing of chains in bulk is tighter; second, the high efficient screening allows greater delocalization of the π (and π^*) orbitals above and below the conjugated framework. Both effects lead to improved interchain “communication”, which leads to an enlarged bandwidth. In the 3D condensed phase, the LCB width is largest along the $\pi - \pi$ stacking compared to any other direction (Figures 3a and 3b) and indicates an efficient band-transport of holes.

The lowest conduction band is very different. The impurity states are strongly localized along the copolymer axis. As a result, local and non-local interactions are insensitive to crystal momentum, and the band is narrow. Further, there are no increased interactions along the $\pi - \pi$ stacking, and the AIB electronic states thus appear to be molecule-like. Hence, the acceptor band is flat along $\Gamma \rightarrow Y$ as well. There is thus a low likelihood of electron band-transport in the face-on or polymer axis directions.

AIB, however, unexpectedly exhibits cooperative effects along the edge-to-edge stacking (Figure 3c). For states near the band minimum (i.e., near Γ), the impurity wavefunction

delocalizes across individual copolymer chains. In contrast, a nodal plane appears between every adjacent polymer for higher crystal momenta due to the increase of the kinetic energy towards the Brillouin zone boundary (i.e., near Z). The associated QP energy variation leads to a relatively wide⁵⁵ dispersion of ~ 300 meV in the $\Gamma \rightarrow Z$ direction. Besides the kinetic contribution, the band widening is also driven by a large variation of the exchange energy. Along $\Gamma \rightarrow Z$, the AIB thus behaves like the conjugated states in the polymer axis. These properties indicate that AIB can sustain electron transport along the edge-to-edge stacking direction.

In summary, we investigated a prototypical example of D-A copolymers, FBT, and explained its electronic structure and the propensity to band transport in the condensed phase. Our many-body calculations are in excellent agreement with available experimental data and, for the first time, they provide insight into the quasiparticle (added hole and electron) states of bulk copolymers. The results show that acceptors, which typically act as strong potential wells for electrons, form a previously unrecognized “impurity” band. In contrast, the donors groups are responsible for delocalized lower (valence) and upper (conduction) conjugated bands. The delocalized states and they surround the acceptor band, but they only mildly affect each other.

The intra-chain transport is negatively impacted by the condensed phase stacking, which affects the rotation between the donor and acceptors. On the other hand, electronic states delocalize across the copolymer strands and form wide bands that likely support efficient transport. Electronic correlations (responsible for the cohesive van der Waals forces) universally suppresses band dispersion, but non-local exchange interactions drive it in selected directions.

The large width of valence bands along the $\pi - \pi$ stacking indicates that hole transport is possible in the face-on direction. Surprisingly, we observe a strong propensity for electron transport along the edge-on stacking within the acceptor impurity band. Hence, D-A copolymers exhibit an orthogonal ambipolar transport network, which has been so far

reported only in heterogeneous mixtures of p-type polymer and a small n-type molecule.^{56,57} Our results suggest that orthogonal transport of electrons and holes can be achieved in pure D-A copolymers merely through molecular packing.

Supporting Information Available

The following files are available free of charge. The Supporting Information provides additional texts, figures and tables listed below.

Texts: computational methods and details.

Figures: 1D, 2D, and 3D supercells in computations, QP energy diagrams of molecular and periodic systems, hybridization of FBT frontier orbitals, selected orbitals of UCB, AIB, and LCB in the 1D system, Comparison of band structures of D-A copolymers with different acceptors, QP band structures with exchange and correlation energy as functions of the momentum, graphical solutions to the QP and correlation energies, representation of the D-A torsion angle.

Tables: parameters in DFT and MBPT calculations, measurements of geometrical constants for different polymers, decomposition of the contribution to the valence bandwidth, bandwidths of the LCB and AIB, exchange contribution to the valence bandwidth, measurements of torsion angle for FBT strands, convergence of the IP, EA, and gap to the supercell's size.

Acknowledgement

The authors want to acknowledge Prof. Thuc-Quyen Nguyen and Prof. Guillermo Bazan for fruitful discussions. This work was supported by the NSF CAREER award through Grant No. DMR-1945098. The calculations were performed as part of the XSEDE computational Project No. TG-CHE180051. Use was made of computational facilities purchased with funds from the National Science Foundation (CNS-1725797) and administered by the Center for

Scientific Computing (CSC). The CSC is supported by the California NanoSystems Institute and the Materials Research Science and Engineering Center (MRSEC; NSF DMR 1720256) at UC Santa Barbara.

References

- (1) Günes, S.; Neugebauer, H.; Sariciftci, N. S. Conjugated Polymer-Based Organic Solar Cells. *Chemical Reviews* **2007**, *107*, 1324–1338.
- (2) Heeger, A. J. Semiconducting polymers: the Third Generation. *Chem. Soc. Rev.* **2010**, *39*, 2354–2371.
- (3) Facchetti, A. π -Conjugated Polymers for Organic Electronics and Photovoltaic Cell Applications. *Chemistry of Materials* **2011**, *23*, 733–758.
- (4) Wang, C.; Dong, H.; Hu, W.; Liu, Y.; Zhu, D. Semiconducting π -Conjugated Systems in Field-Effect Transistors: A Material Odyssey of Organic Electronics. *Chemical Reviews* **2012**, *112*, 2208–2267.
- (5) Yuen, J. D.; Fan, J.; Seifter, J.; Lim, B.; Hufschmid, R.; Heeger, A. J.; Wudl, F. High Performance Weak Donor-Acceptor Polymers in Thin Film Transistors: Effect of the Acceptor on Electronic Properties, Ambipolar Conductivity, Mobility, and Thermal Stability. *Journal of the American Chemical Society* **2011**, *133*, 20799–20807.
- (6) Li, Y. Molecular Design of Photovoltaic Materials for Polymer Solar Cells: Toward Suitable Electronic Energy Levels and Broad Absorption. *Accounts of Chemical Research* **2012**, *45*, 723–733.
- (7) Zhang, X.; Bronstein, H.; Kronemeijer, A. J.; Smith, J.; Kim, Y.; Kline, R. J.; Richter, L. J.; Anthopoulos, T. D.; Sirringhaus, H.; Song, K. et al. Molecular ori-

- gin of high field-effect mobility in an indacenodithiophene-benzothiadiazole copolymer. *Nature Communications* **2013**, *4*, 2238.
- (8) Schwartz, B. J. Conjugated Polymers as Molecular Materials: How Chain Conformation and Film Morphology Influence Energy Transfer and Interchain Interactions. *Annual Review of Physical Chemistry* **2003**, *54*, 141–172, PMID: 12524429.
 - (9) Noriega, R.; Rivnay, J.; Vandewal, K.; Koch, F. P. V.; Stingelin, N.; Smith, P.; Toney, M. F.; Salleo, A. A general relationship between disorder, aggregation and charge transport in conjugated polymers. *Nature Materials* **2013**, *12*, 1038–1044.
 - (10) Oh, J. H.; Lee, H. W.; Mannsfeld, S.; Stoltenberg, R. M.; Jung, E.; Jin, Y. W.; Kim, J. M.; Yoo, J.-B.; Bao, Z. Solution-processed, high-performance n-channel organic microwire transistors. *Proceedings of the National Academy of Sciences* **2009**, *106*, 6065–6070.
 - (11) Barzegar, H. R.; Larsen, C.; Boulanger, N.; Zettl, A.; Edman, L.; Wågberg, T. Self-Assembled PCBM Nanosheets: A Facile Route to Electronic Layer-on-Layer Heterostructures. *Nano Letters* **2018**, *18*, 1442–1447.
 - (12) Sirringhaus, H.; Brown, P. J.; Friend, R. H.; Nielsen, M. M.; Bechgaard, K.; Langeveld-Voss, B. M. W.; Spiering, A. J. H.; Janssen, R. A. J.; Meijer, E. W.; Herwig, P. et al. Two-dimensional charge transport in self-organized, high-mobility conjugated polymers. *Nature* **1999**, *401*, 685–688.
 - (13) Venkateshvaran, D.; Nikolka, M.; Sadhanala, A.; Lemaire, V.; Zelazny, M.; Kepa, M.; Hurhangee, M.; Kronemeijer, A. J.; Pecunia, V.; Nasrallah, I. et al. Approaching disorder-free transport in high-mobility conjugated polymers. *Nature* **2014**, *515*, 384–388.
 - (14) Luo, C.; Kyaw, A. K. K.; Perez, L. A.; Patel, S.; Wang, M.; Grimm, B.; Bazan, G. C.; Kramer, E. J.; Heeger, A. J. General Strategy for Self-Assembly of Highly Oriented

- Nanocrystalline Semiconducting Polymers with High Mobility. *Nano Letters* **2014**, *14*, 2764–2771.
- (15) Li, M.; An, C.; Marszalek, T.; Baumgarten, M.; Yan, H.; Müllen, K.; Pisula, W. Controlling the Surface Organization of Conjugated Donor-Acceptor Polymers by their Aggregation in Solution. *Advanced Materials* **2016**, *28*, 9430–9438.
- (16) Hsu, B. B.-Y.; Cheng, C.-M.; Luo, C.; Patel, S. N.; Zhong, C.; Sun, H.; Sherman, J.; Lee, B. H.; Ying, L.; Wang, M. et al. The Density of States and the Transport Effective Mass in a Highly Oriented Semiconducting Polymer: Electronic Delocalization in 1D. *Advanced Materials* **2015**, *27*, 7759–7765.
- (17) Sakanoue, T.; Sirringhaus, H. Band-like temperature dependence of mobility in a solution-processed organic semiconductor. *Nature Materials* **2010**, *9*, 736–740.
- (18) Yamashita, Y.; Tsurumi, J.; Hinkel, F.; Okada, Y.; Soeda, J.; Zajaczkowski, W.; Baumgarten, M.; Pisula, W.; Matsui, H.; Müllen, K. et al. Transition Between Band and Hopping Transport in Polymer Field-Effect Transistors. *Advanced Materials* **2014**, *26*, 8169–8173.
- (19) Kim, G.; Kang, S.-J.; Dutta, G. K.; Han, Y.-K.; Shin, T. J.; Noh, Y.-Y.; Yang, C. A Thienoisindigo-Naphthalene Polymer with Ultrahigh Mobility of 14.4 cm²/V·s That Substantially Exceeds Benchmark Values for Amorphous Silicon Semiconductors. *Journal of the American Chemical Society* **2014**, *136*, 9477–9483.
- (20) Sutton, C.; Risko, C.; Brédas, J.-L. Noncovalent Intermolecular Interactions in Organic Electronic Materials: Implications for the Molecular Packing vs Electronic Properties of Acenes. *Chemistry of Materials* **2016**, *28*, 3–16.
- (21) Norton, J. E.; Brédas, J.-L. Polarization Energies in Oligoacene Semiconductor Crystals. *Journal of the American Chemical Society* **2008**, *130*, 12377–12384.

- (22) Nayak, P. K.; Periasamy, N. Calculation of electron affinity, ionization potential, transport gap, optical band gap and exciton binding energy of organic solids using solvation model and DFT. *Organic Electronics* **2009**, *10*, 1396–1400.
- (23) Difley, S.; Wang, L.-P.; Yeganeh, S.; Yost, S. R.; Voorhis, T. V. Electronic Properties of Disordered Organic Semiconductors via QM/MM Simulations. *Accounts of Chemical Research* **2010**, *43*, 995–1004.
- (24) Ryno, S. M.; Lee, S. R.; Sears, J. S.; Risko, C.; Brédas, J.-L. Electronic Polarization Effects upon Charge Injection in Oligoacene Molecular Crystals: Description via a Polarizable Force Field. *The Journal of Physical Chemistry C* **2013**, *117*, 13853–13860.
- (25) Refaely-Abramson, S.; Sharifzadeh, S.; Jain, M.; Baer, R.; Neaton, J. B.; Kronik, L. Gap renormalization of molecular crystals from density-functional theory. *Physical Review B* **2013**, *88*, 081204.
- (26) Poelking, C.; Tietze, M.; Elschner, C.; Olthof, S.; Hertel, D.; Baumeier, B.; Würthner, F.; Meerholz, K.; Leo, K.; Andrienko, D. Impact of mesoscale order on open-circuit voltage in organic solar cells. *Nature Materials* **2015**, *14*, 434–439.
- (27) Kang, Y.; Jeon, S. H.; Cho, Y.; Han, S. Ab initio calculation of ionization potential and electron affinity in solid-state organic semiconductors. *Phys. Rev. B* **2016**, *93*, 035131.
- (28) Li, J.; D’Avino, G.; Duchemin, I.; Beljonne, D.; Blase, X. Combining the Many-Body GW Formalism with Classical Polarizable Models: Insights on the Electronic Structure of Molecular Solids. *The Journal of Physical Chemistry Letters* **2016**, *7*, 2814–2820.
- (29) Sun, H.; Ryno, S.; Zhong, C.; Ravva, M. K.; Sun, Z.; Körzdörfer, T.; Brédas, J.-L. Ionization Energies, Electron Affinities, and Polarization Energies of Organic Molecular Crystals: Quantitative Estimations from a Polarizable Continuum Model (PCM)-Tuned Range-Separated Density Functional Approach. *Journal of Chemical Theory and Computation* **2016**, *12*, 2906–2916.

- (30) Li, J.; D’Avino, G.; Duchemin, I.; Beljonne, D.; Blase, X. Accurate description of charged excitations in molecular solids from embedded many-body perturbation theory. *Phys. Rev. B* **2018**, *97*, 035108.
- (31) Bhandari, S.; Cheung, M. S.; Geva, E.; Kronik, L.; Dunietz, B. D. Fundamental Gaps of Condensed-Phase Organic Semiconductors from Single-Molecule Calculations using Polarization-Consistent Optimally Tuned Screened Range-Separated Hybrid Functionals. *Journal of Chemical Theory and Computation* **2018**, *14*, 6287–6294.
- (32) Halls, J. J. M.; Cornil, J.; dos Santos, D. A.; Silbey, R.; Hwang, D.-H.; Holmes, A. B.; Brédas, J. L.; Friend, R. H. Charge- and energy-transfer processes at polymer/polymer interfaces: A joint experimental and theoretical study. *Phys. Rev. B* **1999**, *60*, 5721–5727.
- (33) Cornil, J.; Gueli, I.; Dkhissi, A.; Sancho-Garcia, J. C.; Hennebicq, E.; Calbert, J. P.; Lemaure, V.; Beljonne, D.; Brédas, J. L. Electronic and optical properties of polyfluorene and fluorene-based copolymers: A quantum-chemical characterization. *The Journal of Chemical Physics* **2003**, *118*, 6615–6623.
- (34) Brédas, J. L.; Thémans, B.; Fripiat, J. G.; André, J. M.; Chance, R. R. Highly conducting polyparaphenylene, polypyrrole, and polythiophene chains: An ab initio study of the geometry and electronic-structure modifications upon doping. *Phys. Rev. B* **1984**, *29*, 6761–6773.
- (35) Brédas, J. L.; Street, G. B.; Thémans, B.; André, J. M. Organic polymers based on aromatic rings (polyparaphenylene, polypyrrole, polythiophene): Evolution of the electronic properties as a function of the torsion angle between adjacent rings. *The Journal of Chemical Physics* **1985**, *83*, 1323–1329.
- (36) Cheng, C.; Geng, H.; Yi, Y.; Shuai, Z. Super-exchange-induced high performance charge

- transport in donor-acceptor copolymers. *Journal of Materials Chemistry C* **2017**, *5*, 3247–3253.
- (37) He, F.; Cheng, C.; Geng, H.; Yi, Y.; Shuai, Z. Effect of donor length on electronic structures and charge transport polarity for DTDPP-based D-A copolymers: a computational study based on a super-exchange model. *Journal of Materials Chemistry A* **2018**, *6*, 11985–11993.
- (38) Brédas, J.-L.; Li, Y.; Sun, H.; Zhong, C. Why Can High Charge-Carrier Mobilities be Achieved Along p-Conjugated Polymer Chains with Alternating Donor-Acceptor Moieties? *Advanced Theory and Simulations* **2018**, *1*, 1800016.
- (39) Woods, L. M.; Dalvit, D. A. R.; Tkatchenko, A.; Rodriguez-Lopez, P.; Rodriguez, A. W.; Podgornik, R. Materials perspective on Casimir and van der Waals interactions. *Rev. Mod. Phys.* **2016**, *88*, 045003.
- (40) Martin, R. M.; Reining, L.; Ceperley, D. M. *Interacting Electrons: Theory and Computational Approaches*; Cambridge University Press, 2016.
- (41) Neuhauser, D.; Gao, Y.; Arntsen, C.; Karshenas, C.; Rabani, E.; Baer, R. Breaking the Theoretical Scaling Limit for Predicting Quasiparticle Energies: The Stochastic GW Approach. *Phys. Rev. Lett.* **2014**, *113*, 076402.
- (42) Vlček, V.; Rabani, E.; Neuhauser, D.; Baer, R. Stochastic GW Calculations for Molecules. *Journal of Chemical Theory and Computation* **2017**, *13*, 4997–5003, PMID: 28876912.
- (43) Vlček, V.; Li, W.; Baer, R.; Rabani, E.; Neuhauser, D. Swift GW beyond 10,000 electrons using sparse stochastic compression. *Phys. Rev. B* **2018**, *98*, 075107.
- (44) Vlček, V. Stochastic Vertex Corrections: Linear Scaling Methods for Accurate Quasiparticle Energies. *Journal of Chemical Theory and Computation* **2019**, *15*, 6254–6266.

- (45) Blase, X.; Attaccalite, C.; Olevano, V. First-principles *GW* calculations for fullerenes, porphyrins, phtalocyanine, and other molecules of interest for organic photovoltaic applications. *Phys. Rev. B* **2011**, *83*, 115103.
- (46) Mai, C.-K.; Zhou, H.; Zhang, Y.; Henson, Z. B.; Nguyen, T.-Q.; Heeger, A. J.; Bazan, G. C. Facile Doping of Anionic Narrow-Band-Gap Conjugated Polyelectrolytes During Dialysis. *Angewandte Chemie International Edition* **2013**, *52*, 12874–12878.
- (47) Mai, C.-K.; Russ, B.; Fronk, S. L.; Hu, N.; Chan-Park, M. B.; Urban, J. J.; Segalman, R. A.; Chabinyk, M. L.; Bazan, G. C. Varying the ionic functionalities of conjugated polyelectrolytes leads to both p- and n-type carbon nanotube composites for flexible thermoelectrics. *Energy & Environmental Science* **2015**, *8*, 2341–2346.
- (48) Cui, Q.; Bazan, G. C. Narrow Band Gap Conjugated Polyelectrolytes. *Accounts of Chemical Research* **2018**, *51*, 202–211.
- (49) Zhou, H.; Yang, L.; You, W. Rational Design of High Performance Conjugated Polymers for Organic Solar Cells. *Macromolecules* **2012**, *45*, 607–632.
- (50) Duan, C.; Huang, F.; Cao, Y. Recent development of push-pull conjugated polymers for bulk-heterojunction photovoltaics: rational design and fine tailoring of molecular structures. *Journal of Materials Chemistry* **2012**, *22*, 10416–10434.
- (51) The one-body terms include the single particle non-interacting kinetic energy and external as well as the Hartree potential energies.
- (52) The external and Hartree potentials are manifestedly local; the non-interacting kinetic energy is determined purely by a Kohn-Sham map using a local potential. Note that the many-body calculations use a perturbative correction with the Kohn-Sham results as a starting point. The non-local contributions are included in the self-energy term, i.e., it is part of the electron-electron interaction.

- (53) Mori-Sánchez, P.; Cohen, A. J.; Yang, W. Localization and Delocalization Errors in Density Functional Theory and Implications for Band-Gap Prediction. *Phys. Rev. Lett.* **2008**, *100*, 146401.
- (54) Vlček, V.; Eisenberg, H. R.; Steinle-Neumann, G.; Neuhauser, D.; Rabani, E.; Baer, R. Spontaneous Charge Carrier Localization in Extended One-Dimensional Systems. *Phys. Rev. Lett.* **2016**, *116*, 186401.
- (55) For comparison, this value is practically identical to the dispersion of the conjugated bands along the polymer chain in the 2D system (c.f., Figure ??).
- (56) Huang, W.; Markwart, J. C.; Briseno, A. L.; Hayward, R. C. Orthogonal Ambipolar Semiconductor Nanostructures for Complementary Logic Gates. *ACS Nano* **2016**, *10*, 8610–8619.
- (57) Huang, W.; Hayward, R. C. Orthogonal Ambipolar Semiconductors with Inherently Multi-Dimensional Responses for the Discriminative Sensing of Chemical Vapors. *ACS Applied Materials & Interfaces* **2018**, *10*, 33353–33359.